Position Locking for Permanent Magnet Synchronous Machine Propeller Drives in Drones by Hall-Effect Sensor-Assisted Nonlinear Observer

Emil Jenssen[1] Kristoffer Gryte[1] Jon Are Suul[1,2]
[1]Department of Engineering Cybernetics, Norwegian University of Science and Technology, Trondheim, Norway
[2]SINTEF Energy Research, Trondheim, Norway
e-mail: emiljen@stud.ntnu.no, kristoffer.gryte@ntnu.no, jon.are.suul@ntnu.no

***Abstract*—The paper presents a hall-effect sensor-assisted nonlinear observer-based solution for position locking of a surface-mounted permanent magnet synchronous motor (SMPMSM) propeller drive in drone applications. The purpose of the position locking is to ensure a fixed motor position at the landing instant to avoid mechanical damage to the propeller. To evaluate the proposed solution, the position locking sequence of the motor drive is studied for two cases, implemented with two different state machines. The first case is relying on an encoder to provide the position feedback signal and serves as a reference for assessing the performance of the proposed solution based on the position estimate from the hall-effect sensor-assisted nonlinear observer. Experimental results show how the proposed solution can provide sufficient performance of position locking without the encoder.**

***Index Terms*—Encoder-less position control, hall-effect sensor, nonlinear observer, permanent magnet synchronous machine, position locking, position control, propeller drive, state machine**

I. Introduction

FIXED-WING unmanned aerial vehicles (UAVs) require minimal drag for ensuring long endurance. The lower the landing gear, the less drag it creates, which helps to increase endurance and range. However, low landing gear increases the risk of the propulsion propeller hitting the ground and being damaged during landing. Thus, the balance between low landing gear profile and drag increase is a challenge for designers. Alternative solutions for avoiding damage is the use of flexible propellers [1] or foldable blades for underwater gliders [2]. Even so, the orientation of the blades and the corresponding mitigation of risk when landing is uncertain. Instead, locking the rotor position with the propeller blades in a horizontal orientation gives the possibility to minimize the landing gear to improve the overall efficiency of the UAV. This implies the need for position locking control by the propeller drive during landing of the UAV.

Another application where position locking is useful is hovering motors in vertical take-off and landing (VTOL) vehicles. These motors are only active in the take-off and landing phases, and the drag forces during cruise can be reduced by aligning the propeller blades with the heading angle. This technology has been demonstrated by the industry [3]–[5], but to the best of our knowledge, no implementations have been presented in the open literature.

Using an encoder is an established solution for position control in electric motor drives [6], [7]. However the addition of an encoder in low cost UAV drive systems increases the cost and imply the need for additional maintenance due to wear. Thus, solutions for minimizing, or possibly removing the sensoring requirements are desirable.

The most common choice of motor for UAVs is the surface-mounted permanent-magnet synchronous motor (SMPMSM) due to the high efficiency and high power density [8], [9]. However, sensorless control of permanent-magnet synchronous motors (PMSMs) generally include two main groups of methods [10], [11]. One group includes the model-based approaches, such as back electromotive force (EMF) and observer based methods [12]–[15]. These methods provide good performance at the medium to high speed range. The other group is the saliency-based methods, such as the high frequency injection (HFI) method, which provide capability for position estimation in the low speed range [16]–[18].

Applying a sensorless control method to remove the encoder and simplifying the sensor hardware is a natural choice for reducing cost of the propeller drive in a drone. However, saliency-based methods are not feasible for non-salient PMSMs. Furthermore, the model-based non-linear observer proposed for position estimation in [15] is not applicable at zero speed [19]. To achieve encoder-less position locking of the propeller drive system, a solution relying on a nonlinear observer supported by a single hall-effect sensor is studied in this paper. For this purpose two state machines with different types of position feedback, including a reference case with encoder-based control, are presented and compared by experimental tests. Although the precision and flexibility is reduced compared to encoder-based control, the results show that the hall-effect sensor-assisted control can provide sufficient capability for locking the propeller in a specific position.

II. Position Estimation and Hall-sensor

In addition to the use of an encoder as a position sensor, several methods can identify the rotor position.

This research was funded by the Research Council of Norway through the *Regionale forskningsfond* funding scheme, grant number 328510.

A. Sensorless Control

The sensorless control proposed by [15] is used as a starting point in this paper, and relies on field-oriented control (FOC) with a speed observer and a nonlinear observer for position estimation. The sensorless control is based on the electrical and mechanical dynamics of the SMPMSM, as represented in the stationary $\alpha\beta$ reference frame by:

$$L\frac{di_{\alpha\beta}}{dt} = -R_s i_{\alpha\beta} + \omega\psi_m \begin{bmatrix} sin\theta \\ -cos\theta \end{bmatrix} + v_{\alpha\beta} \tag{1a}$$

$$T_e = \frac{3}{2}\frac{P}{2}\psi_m(i_\alpha cos\theta - i_\beta sin\theta) \tag{1b}$$

where $i_{\alpha\beta} = \begin{bmatrix} i_\alpha & i_\beta \end{bmatrix}^\intercal$ is the stator current, and $v_{\alpha\beta} = \begin{bmatrix} v_\alpha & v_\beta \end{bmatrix}^\intercal$ is the stator voltage. Furthermore, R_s is the stator resistance and L is the stator inductance, which is constant and independent of the rotor angle θ. The phase resistance is $r_s = \frac{2}{3}R_s$ and the phase inductance is $l_s = \frac{2}{3}L$. The constant permanent-magnet flux linkage is ψ_m, and T_e is the electromagnetic torque. The electrical rotor angle is given by $\theta = \frac{P}{2}\theta_r$, where θ_r is the mechanical rotor angle, and P is the number of motor poles.

The electrical rotor speed relates to the electrical rotor angle as $\omega = \frac{d\theta}{dt}$, and the mechanical rotor speed is $\omega_r = \frac{1}{P/2}\omega$. The electrical dynamic of the SMPMSM is transformed to the synchronous dq reference frame to be applicable in the sensorless FOC, as given by

$$L\frac{di_d}{dt} = -R_s i_d + \omega L i_q + v_d \tag{2a}$$

$$L\frac{di_q}{dt} = -R_s i_q - \omega L i_d - \omega\psi_m + v_q \tag{2b}$$

where $i_{dq} = \begin{bmatrix} i_d & i_q \end{bmatrix}^\intercal$ and $v_{dq} = \begin{bmatrix} v_d & v_q \end{bmatrix}^\intercal$.

The nonlinear observer for position estimation is based on the state variables given in (3). Note that $x = \begin{bmatrix} x_1 & x_2 \end{bmatrix}^\intercal$.

$$x = Li_{\alpha\beta} + \psi_m \begin{bmatrix} cos\theta \\ sin\theta \end{bmatrix} \tag{3}$$

By rearranging (3), the estimated position $\hat{\theta}$ is given by

$$\hat{\theta} = tan^{-1}\left(\frac{\hat{x_2} - Li_\beta}{\hat{x_1} - Li_\alpha}\right) \tag{4}$$

where $\hat{x} = \begin{bmatrix} \hat{x_1} & \hat{x_2} \end{bmatrix}^\intercal$ is the estimated state variable. The nonlinear observer is simple to implement with only one observer gain $\gamma > 0$ to tune. However, at zero speed, the vector x is proven not observable. Further detailed information on the design of the nonlinear observer and its stability properties is available in [15], [19].

The speed observer is constructed as a tracking-controller-type on the form shown in (5), and yields an estimated speed necessary as a feedback variable for the sensorless control [20].Here, K_p and K_i are the proportional and integral gains, respectively. The input is the estimated position $\hat{\theta}$, which is tracked by z_1, yielding an estimated speed $\hat{\omega} = \dot{z_1}$.

$$\hat{\omega} = \dot{z_1} = K_p\dot{z_2} + K_i z_2, \quad \dot{z_2} = \hat{\theta} - z_1 \tag{5}$$

B. Hall-effect Sensor

The studied low cost encoder-less solution applies a hall-effect sensor integrated into the stator and a magnet mounted on the rotor to represents a fixed reference point. The pulled-up signal illustrated in fig. 1 shows how the signal falls low when the magnet is close to the sensor and triggers an interrupt for precise indexing of the rotor at one consistent position.

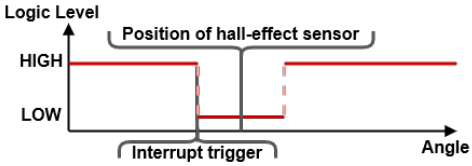

Fig. 1. A concept of the hall-effect sensor signal.

III. Proposed System Structure and Design

The applied control system is divided into three loops, the inner, outer, and state machine loop, as shown in fig. 2. The inner loop is the sensorless control with FOC, speed observer, and nonlinear observer for position estimation, which feeds the phase voltage references v_{abc} to the pulse-width modulated (PWM) inverter driving the motor. The phase currents i_{ab} are measured and transformed to i_{dq} for the FOC and nonlinear observer. For detailed information, see [15].

The outer loop provides a current reference i_q^* as input for the FOC from a selected control mode, such as a position or speed controller, as defined by the state machine.

The state machine loop receives a throttle signal as input, and chooses a control mode according to the speed and position as well as the current state of the state machine. The estimated speed is received from the speed observer, and position information is provided by either an encoder or as the modified nonlinear observer position (MNOP) supported by the hall-effect sensor.

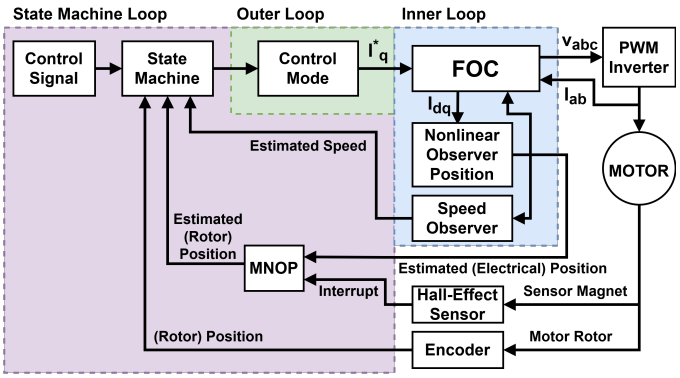

Fig. 2. System block diagram with the inner, outer, and state machine loops.

The nonlinear observer for position estimation is based on the electrical position and requires modifications to yield the mechanical position. For instance, when an eight pole motor have completed one revolution, the observer sees it as four revolutions. Thus, mapping the estimated position with the

pole-pairs $\frac{P}{2}$ as the ratio yields a estimation of the mechanical position.

To ensure the estimated position is consistent with the mechanical orientation, the hall-effect sensor is utilized as a correction for the position estimation. In addition, an offset for reverse direction is added since the interrupt triggers at a different position when the motor rotates in the opposite direction. Further detailed information is presented in [21]. The sign of the estimated speed is used to indicate rotor direction for applying the offset. This ensures a consistent estimation of the mechanical position. Note that the non-observability at zero speed persists.

IV. State Machines

A. PID Position Control State Machine

The proportional–integral–derivative (PID) position control (PPC) state machine is shown in fig. 3. It is designed to utilize a PID controller in the outer loop for converging to and holding the rotor in the desired position in the *PID position control* state. The PID controller requires a feedback of the position, e.g. with an encoder. The regular speed control mode corresponds to the *duty cycle (D.C.) control* state. In this mode, the system uses the current controller in the FOC to change the rotor speed, with a D.C. value as an input in relation to predefined current limits. The *current brake* state is a transient state to slow down the motor for smoother transition by changing from speed control to position control at a lower speed. The *idle* state is the initial and temporary state for when the motor is not excited and not in need of neither speed or position control. When the throttle is above zero, the state machine changes to the *D.C. control* state from all the states, and when throttle is zero in the *D.C. control* state it transitions to the *current brake* state, until the speed is low enough to transition to the *PID position control* state. The system returns to the *idle* state after an arbitrary time in the *PID position control* state.

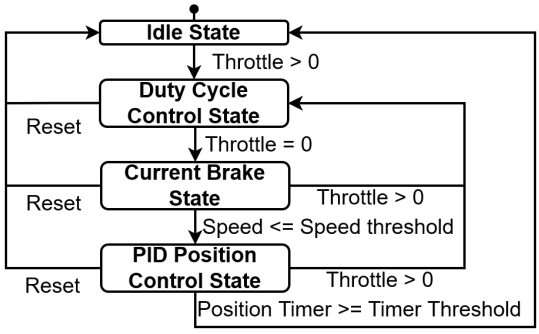

Fig. 3. A flow diagram of the PID position control state machine.

B. Position Hold State Machine

The position hold (PH) state machine is shown in fig. 4. The *idle* and *D.C. control* states are the same as for the PPC state machine. However, the *rotation* and *position hold* states correspond to position locking, and are independent of PID controller logic and a position sensor such as an encoder. The PH state machine is still dependent on a reference signal to stop at a consistent position. The rotation state slows down the motor to a slow and constant speed. The *position hold* state feds the motor phases with a constant current, locking the rotor position in alignment with the motor poles-pairs when the conditions for position locking are met with a margin at slow speed. The modified nonlinear observer position estimation with the hall-effect sensor is suitable to lock the rotor consistently at any desired position, since the state machine avoids zero speed operation before the position is being locked.

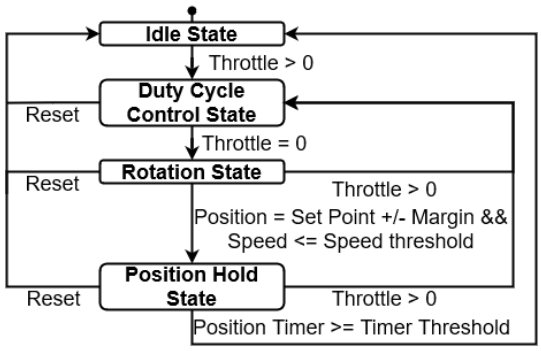

Fig. 4. A flow diagram of the position hold state machine.

V. Test Setup and Experimental Results

The experiments were performed on the test setup in fig. 5a. On the right hand is a SMPMSM with a propeller, encoder, hall-effect sensor, and the motor controller. The hall-effect sensor is shown in fig. 5b, with the hall-effect sensor (red solid circle) fixed to the stator, and two magnets (red dashed circles) on the rotor. Only one magnet is detectable due to incorrect magnetic polarity introduced on the sensor. The encoder is fixed to the bracket and the sleeve to the rotor shaft (blue solid circle). On the left hand side, a motor with a propeller introduces a wind disturbance on the system.

The motor controller is a VESC 6 MkV. It was chosen for the customization capabilities and its already existing solutions for incremental encoder reading. The sensorless control with the speed observer and the nonlinear observer algorithm from [15] was also available. The state machine loop was implemented directly into the firmware of the motor controller, with the parameters listed in table I.

A summary of 30 experiments for both state machines with 20m/s wind disturbance is listed in table III, and shows the normal distribution of the steady-state position wrapped to [-180 180] degrees, and the settling time (ST) with 1% ST threshold, corresponding to ± 2 degrees. The PH state machine has a larger standard deviation of the steady-state position and a faster settling time in comparison to the PPC state machine. The experiments are conducted with the same control signal set to 70% for speed control at approximately 1900rpm, and then to 0% for position control.

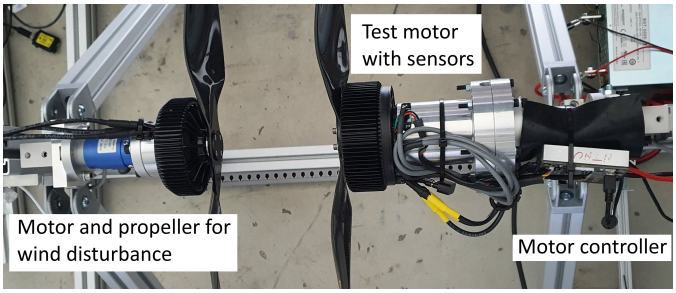

(a)

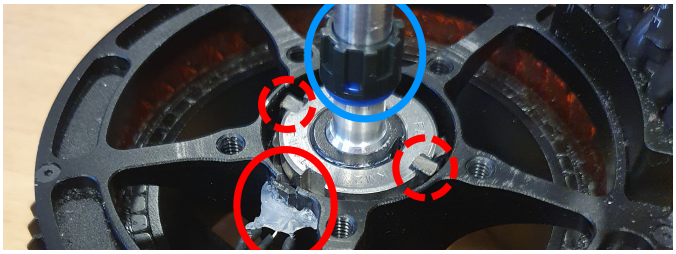

(b)

Fig. 5. Pictures of the experiment setup. (a) The test setup. (b) Back side of the motor hub with the hall-effect sensor and magnets (red), and the encoder sleeve (blue).

TABLE I
PARAMETERS OF SMPMSM AND SENSORLESS CONTROL FOR EXPERIMENTS

Parameters [unit]	Values
Input DC voltage [V]	22.2
Rated nominal power [kW]	1.1
Rated peak power [kW]	3.1
Rotor inertia [kgm^2]	0.002
Number of poles (P)	28
Back-EMF constant star-connection [V/krpm]	8.03 (peak, line-to-line)
Switching frequency [kHz]	25
Motor resistance (R_s) [mΩ]	21.7
Motor inductance (L) [μH]	2.83
Inductance difference (Ld - Lq) [μH]	0.17
Rotor flux linkage (ψ_m) [mWb]	2.868
Current proportional gain (K_P)	0.0003
Current integral gain (K_I)	2.17
Position observer gain (x1M) (γ)	121.57
Speed observer proportional gain (K_P)	2000
Speed observer integral gain (K_I)	30000

A. PID Postion Control State Machine with Encoder

The experiments of the PPC state machine are conducted with the parameters listed in table II. Figure 6 shows results from one experiment, including speed, control signal and position, with the states divided into separate regions. In the *idle state* region, the motor is not excited but still above zero speed due to the wind disturbance. The speed control is activated in the *D.C. control state* region while the control signal is above zero. The control signal is set back to zero at 1200ms, and enters the *current brake state* region with the motor slowing down. The braking is relative slow due to a low *relative current brake* value of 20%, and could be increased for reducing the settling time. In the *PID position control state* region the PID controller converges the position to a set point at zero degrees. The encoder reading of all the 30 experiments in fig. 7 shows consistent convergence of the position.

The distribution of the steady-state position is represented with a normal distribution in fig. 8a, and shows consistency with one exception at approx. -1.8 degrees. This is possibly due to uneven wind disturbance and indicates no risk of hitting the ground during landing, as there is a margin of error in the position. The distribution of the settling time is represented with a normal distribution in fig. 8b and defined from the moment when the control signal is set to zero at 1200ms. The exception from the position distribution is seen with a settling time of approximately 1400ms, and suggests a critical scenario if the transition from throttling to touch-down is less. Nonetheless, the ST threshold is strict in comparison to the propeller drive application and should not be at risk within 1400ms.

TABLE II
PARAMETERS FOR THE PPC STATE MACHINE

Parameters [unit]	Values
Current brake speed threshold [rpm]	800
Current limit [A]	67.11
Relative current brake [%]	20
PID position control loop rate [Hz]	1000
Position proportional gain (K_P)	0.01
Position integral gain (K_I)	0.06
Position derivatie gain (K_D)	0.0006
Position derivative filter	0.2
Position PID offset angle [degrees]	77.70
PID set point (encoder) [degrees]	0.0
Encoder offset [degrees]	61.8
Encoder ratio	14

TABLE III
A SUMMARY OF THE EXPERIMENTS

State machine		Position (degrees)		Settling time (ms)	
Type	Feedback	μ (mean)	σ (SD)	μ (mean)	σ (SD)
PPC	Encoder	-0.311	0.292	1163.36	81.48
PH	MNOP	-64.936[a]	4.645	846.71	72.04

[a]From the encoder reading. The encoder is not used as a feedback, and only the standard deviation should be used for comparison of the solutions.

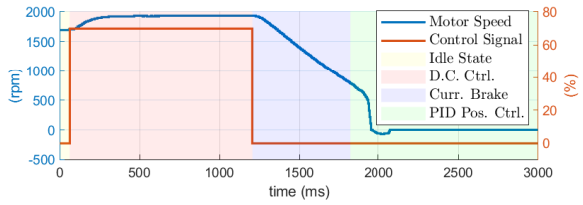

(a)

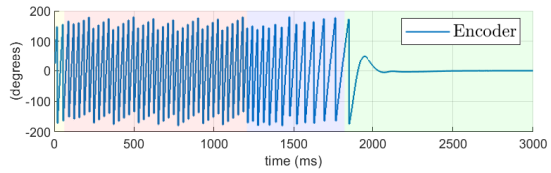

(b)

Fig. 6. An experiment of the PPC state machine with encoder. (a) Speed and control signal. (b) Encoder position.

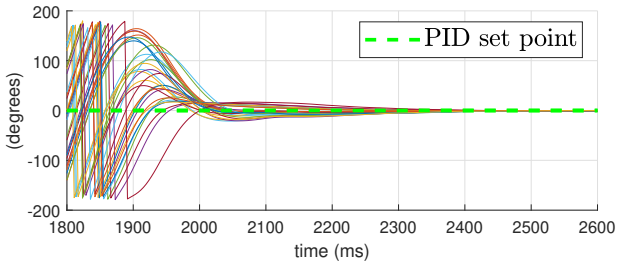

Fig. 7. Comparison of 30 experiments showing convergence of position for PPC state machine with encoder.

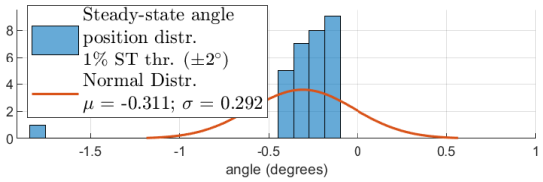

(a)

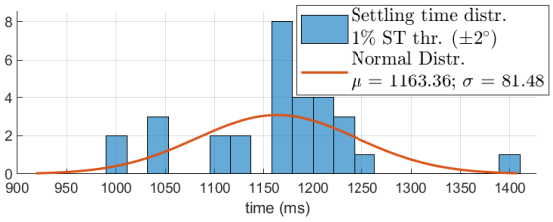

(b)

Fig. 8. Distribution of (a) the steady-state position and (b) the settling time for 30 experiments of the PPC state machine.

B. Position Hold State Machine with MNOP

The experiments of the PH state machine are conducted with the parameters listed in table IV. Note that the set point correlates to the MNOP feedback, and not the reading of the encoder. Figure 9 shows one experiment with speed, control signal and position reading from the encoder and MNOP. The *idle state* and *D.C. control state* regions behave the same as with the PPC state machine. The *rotation state* region drops the motor speed down to about 280rpm with a constant input. When the conditions for the speed and position are met it enters the *position hold state* region and the motor is locked into position with a constant current to the motor phases. From the position readings, in the beginning of the *D.C. control state* and *rotation state* regions there is a change in the difference between the MNOP and encoder with a step of 51.5 degrees, which is due to an undesirable behaviour of the correction with the index offset for reverse directions. Nonetheless, the difference is corrected again before transitioning to the *position hold state* region. The MNOP collapses in the *position hold* region due to non-observability at zero speed.

The encoder readings from all the 30 experiments are compared in fig. 10 and shows a deviation due to a non-strict *rotation speed threshold* value. In comparison to the PPC state machine, the PH state machine is not able to converge to all the set points that the PID controller can follow. Instead, it is limited by how the motor locks into position with the motor poles in the *position hold state* region. In this state, the constant current aligns the rotor with the motor pole-pairs, yielding 14 possible positions for a 28 poles motor. This results in a constant deviation if the Hall-effect sensor is not mounted accordingly to the pole-orientation. The set point for the MNOP was derived from experiments with a set of different set points resulting in the same locking position, and choosing the median value for a consistent position.

Another aspect seen from the results is how the PH state machine differs from the PPC state machine. The PID controller is continuously minimizing the risk of damage on the propeller since the position converges to the set point. The PH state machine on the other hand does not have control of the position until the moment it is locked. In other words, if speed of response is important, the PH state machine has a higher risk of spinning the propeller for longer.

The distribution of the steady-state position is represented with a normal distribution in fig. 11a, which shows that all the experiments locks to the same position, with one exception for the abnormality at approximately -42 degrees due to the position locking method and a non-strict threshold. The distribution of settling time in fig. 11 shows consistency, even with the abnormality at a different steady-state position. Note that the PH state machine settles faster than the PPC state machine. However, there is room for improvement of the settling time for the PPC state machine.

TABLE IV
PARAMETERS FOR THE PH STATE MACHINE

Parameters [unit]	Values
Rotation speed threshold [rpm]	400
Rotation duty cycle [%]	10[a]
Position hold current [A]	15
MNOP Set point [degrees]	88.0[b]
MNOP Position margin [degrees]	1.0
MNOP Index offset [degrees]	51.5

[a]Approximately 280 [rpm], [b]No correlation to encoder reading

VI. CONCLUSION

Two state machines have been presented for position locking of a SMPMSM propeller drive. The proposed implementation with a nonlinear observer and a simple hardware alternative to an encoder is compared with the reference design utilizing an encoder and a PID controller. The characteristics of the nonlinear observer prevents controlled stops to zero speed by a PID controller, and the position locking solution in the PH state machine only allows for a limited amount of lockable positions. Thus, the proposed solution requires a mounting procedure that aligns the motor hub with the motor poles in the UAV but provides sufficient performance to ensure landing with the propeller locked in a safe position.

ACKNOWLEDGMENT

The authors thanks A. Matveev, K. K. Nielsen, and A. Franzén at Alva Industries for discussions, use of facility

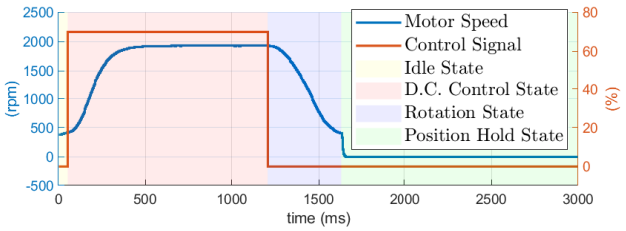

(a)

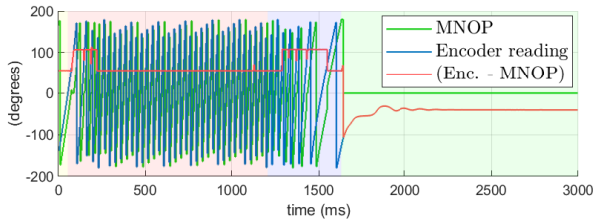

(b)

Fig. 9. An experiment of the PH state machine with MNOP. (a) Speed and control signal. (b) Position reading from encoder.

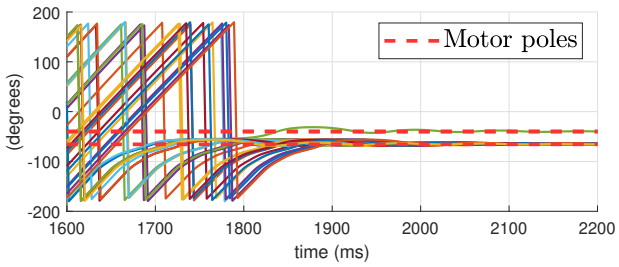

Fig. 10. Comparison of 30 experiments showing convergence of position for PH state machine with MNOP.

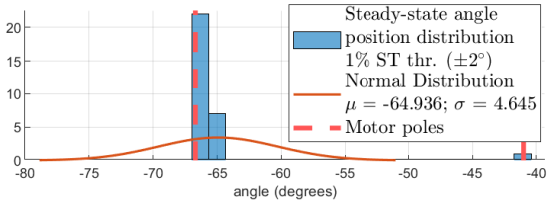

(a) Steady-state angle

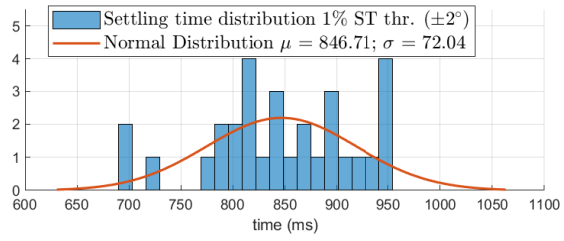

(b) Settling time

Fig. 11. Distribution of (a) the steady-state position and (b) the settling time for 30 experiments of the PH state machine with MNOP.

and equipment, and T. Houge and M. F. Cañas at Maritime Robotics for discussions on design and implementation.

References

[1] D. Q. Nguyen, G. Loianno, and V. A. Ho, "Towards design of a deformable propeller for drone safety," in *2020 3rd IEEE Int. Conf. on Soft Robot. (RoboSoft)*, 2020, pp. 464–469.

[2] Z. Chen, J. Yu, A. Zhang, R. Yi, and Q. Zhang, "Folding propeller design and analysis for a hybrid driven underwater glider," in *2013 OCEANS - San Diego*, 2013, pp. 1–9.

[3] Edge Autonomy, "Penguin C MIL VTOL Fixed-Wing UAS - presentation video 2021," Available: https://youtu.be/pV9iXIa6E9Y [Accessed: 27.05.2022].

[4] T-MOTOR FOR UAV DRONE, "locking propeller at the right position of VTOL drone," Available: https://youtu.be/madW6zLihS8 [Accessed: 27.05.2022].

[5] Textronsystems, "Aerosonde® HQ Advantages," Available: https://youtu.be/hL25olrrvps [Accessed: 27.05.2022].

[6] S. Wekhande and V. Agarwal, "High resolution absolute position vernier shaft encoder suitable for high performance PMSM servo drives," in *PESC 98 Record. 29th Annual IEEE Power Electron. Specialists Conf. (Cat. No.98CH36196)*, vol. 1, 1998, pp. 119–124 vol.1.

[7] Y.-S. Kung and P.-G. Huang, "High performance position controller for PMSM drives based on TMS320F2812 DSP," in *Proc. of the 2004 IEEE Int. Conf. on Contr. Appl., 2004.*, vol. 1, 2004, pp. 290–295 Vol.1.

[8] S. Sakunthala, R. Kiranmayi, and P. N. Mandadi, "A study on industrial motor drives: Comparison and applications of pmsm and bldc motor drives," in *2017 Int. Conf. on Energy, Commun., Data Analytics and Soft Comput. (ICECDS)*, 2017, pp. 537–540.

[9] M. Miyamasu and K. Akatsu, "Efficiency comparison between brushless DC motor and brushless AC motor considering driving method and machine design," in *IECON 2011 - 37th Annu. Conf. of the IEEE Ind. Electron. Soc.*, 2011, pp. 1830–1835.

[10] G. Wang, M. Valla, and J. Solsona, "Position sensorless permanent magnet synchronous machine drives—a review," *IEEE Trans. on Ind. Electron.*, vol. 67, no. 7, pp. 5830–5842, 2020.

[11] P. Acarnley and J. Watson, "Review of position-sensorless operation of brushless permanent-magnet machines," *IEEE Trans. on Ind. Electron.*, vol. 53, no. 2, pp. 352–362, 2006.

[12] N. Matsui, "Sensorless PM brushless DC motor drives," *IEEE Trans. on Ind. Electron.*, vol. 43, no. 2, pp. 300–308, 1996.

[13] J. Solsona, M. Valla, and C. Muravchik, "A nonlinear reduced order observer for permanent magnet synchronous motors," in *Proc. of IECON'94 - 20th Annu. Conf. of IEEE Ind. Electron.*, vol. 1, 1994, pp. 38–43 vol.1.

[14] M. Jansson, L. Harnefors, O. Wallmark, and M. Leksell, "Synchronization at startup and stable rotation reversal of sensorless nonsalient PMSM drives," *IEEE Trans. on Ind. Electron.*, vol. 53, no. 2, pp. 379–387, 2006.

[15] J. Lee, J. Hong, K. Nam, R. Ortega, L. Praly, and A. Astolfi, "Sensorless control of surface-mount permanent-magnet synchronous motors based on a nonlinear observer," *IEEE Trans. on power electron.*, vol. 25, no. 2, pp. 290–297, 2009.

[16] N. Bianchi, S. Bolognani, J.-H. Jang, and S.-K. Sul, "Comparison of PM motor structures and sensorless control techniques for zero-speed rotor position detection," in *2006 37th IEEE Power Electron. Specialists Conf.*, 2006, pp. 1–7.

[17] M. Corley and R. Lorenz, "Rotor position and velocity estimation for a salient-pole permanent magnet synchronous machine at standstill and high speeds," *IEEE Trans. Ind. Appl.*, vol. 34, no. 4, pp. 784–789, 1998.

[18] T. Aihara, A. Toba, T. Yanase, A. Mashimo, and K. Endo, "Sensorless torque control of salient-pole synchronous motor at zero-speed operation," *IEEE Trans. Power Electron.*, vol. 14, no. 1, pp. 202–208, 1999.

[19] R. Ortega, L. Praly, A. Astolfi, J. Lee, and K. Nam, "Estimation of rotor position and speed of permanent magnet synchronous motors with guaranteed stability," *IEEE Trans. on Contr. Syst. Technol.*, vol. 19, no. 3, pp. 601–614, 2011.

[20] S. Morimoto, K. Kawamoto, M. Sanada, and Y. Takeda, "Sensorless control strategy for salient-pole PMSM based on extended EMF in rotating reference frame," *IEEE Tran. on Ind. Appl.*, vol. 38, no. 4, pp. 1054–1061, 2002.

[21] E. Jenssen, "Position control and locking of permanent magnet synchronous motor for propeller drives in drones," M.S. Thesis, Dept. of Eng. Cybern., NTNU, Trondheim, Norway, 2022.